Applied Thermal Engineering 206 (2022) 118040

Contents lists available at ScienceDirect

Applied Thermal Engineering

journal homepage: www.elsevier.com/locate/apthermeng

Performance optimisation of microchannel pin-fins using 2D CFD

Justina Jaseliūnaitė *, Marijus Šeporaitis

Laboratory of Nuclear Installation Safety, Lithuanian Energy Institute, Breslaujos Str. 3, LT-44403 Kaunas, Lithuania

ARTICLE INFO

Keywords:
Microchannel
Pin-fins
Computational fluid dynamics
Complex flow
Hydraulic performance

ABSTRACT

As electronic devices become smaller, they need modern and efficient heat removal solutions. One such solution is microchannel arrays, where the flow around the pin-fins improves heat transfer. However, there is still no consensus on the best array configuration. This numerical study, therefore, focuses on the effect of pin-fins geometry, spacing, and arrangement on performance. Pressure drop and flow characteristics were investigated for 20 different inline and staggered layouts with circular or elliptical pin-fins. The results show that the diameter of the pins has an influence on the strength of the vortices. Larger diameters lead to flow stabilisation and lower pressure drop, while smaller diameters lead to stronger vortex shedding and higher pressure drop. In addition, the flow is more stable when the pin-fins are staggered and closely spaced. This behaviour can be attributed to the greater influence of the cross-sectional area than the meandering of the flow. Finally, the optimum performance was attained using the S-Dx100-Dy40-Px200-Py120 case.

1. Introduction

The electronics industry growth continues with the improvement in manufacturing techniques which provide a significant reduction in the size of the components. Nevertheless, as nanoelectronics manufacturing reaches new limits, the underlying problem of heat dissipation is becoming more and more challenging. Operating temperature affects the reliability of electronics, thus temperature related failures like overheating, non-uniform temperature distribution, and hotspots are the leading cause of the shortened life span of electronic chips and their permanent damage [1,2].

In-chip interlayer cooling using microchannels has a compact structure, is lightweight, can dissipate heat from hot spots preventing local damage , making it an attractive thermal management method for electronic chips [3]. Pin or plate finned microchannel heat sinks enhance heat transfer even more compared to the plane microchannels [2,4]. Obstructed geometry promotes boundary layer disruption, moreover, it induces flow disturbances and vortex formation, which enhance fluid mixing [3]. Furthermore, the increased surface-to-volume ratio provides a larger heat transfer area. Williamson [5] and Žukauskas [6] show, that flow around a cylinder is laminar and has a two-vortex recirculation region till $Re < 49$. At $49 < Re < 140–194$ the flow becomes unstable, mainly due to von Karman vortices. The vortex shedding causes fluctuations in the aerodynamic and pressure field around the obstacle and the heat transfer rate also fluctuates. An even higher *Re* number leads to a wake-transition regime and turbulence, which enhances heat transfer and also increases the pressure drop. The previous studies have been complimented by Alfieri et al. [7], which investigated the flow over the single row of pins. In general, more obstacles create more possibilities for the flow to become unstable. In addition, some experimental studies have concluded that flow in pin-finned microchannel experiences faster and more intense flow disturbances, detachments, and vortices than flow in a circular pipe [8,9]. However, while the *Re* number is well suited for comparing flows, it is not a clear indicator of localised turbulence, which is actually caused not by inertial forces, but by shear forces due to the flow's interaction with the surfaces that bound it [10].

Optimization of the microchannel heat sink performance can be done with respect to the structural materials, flow conditions, coolants, channel geometries. A number of numerical and experimental studies have been conducted in order to optimize and enhance the removal of heat from electronic devices as well as to reduce pressure drop. Several researchers have attempted to improve the thermohydraulic characteristics by changing pin–fin shape. Ambreen et al. [11] analysed the fin shape impact on the heat transfer at the range of Reynolds number (*Re*) $250 \leq Re \leq 550$ and used nano-fluids and water as a coolant. Their results showed that the configuration of circular cross-section fins gives the highest thermal performance, while the hexagon and square fins have lower thermal performance due to the earlier flow separation. In another work, Ambreen et al. [12,13], again numerically found that

* Corresponding author.
E-mail addresses: Justina.Jaseliunaite@lei.lt (J. Jaseliūnaitė), Marijus.Seporaitis@lei.lt (M. Šeporaitis).

https://doi.org/10.1016/j.applthermaleng.2022.118040
Received 16 August 2021; Received in revised form 22 November 2021; Accepted 4 January 2022
Available online 15 January 2022

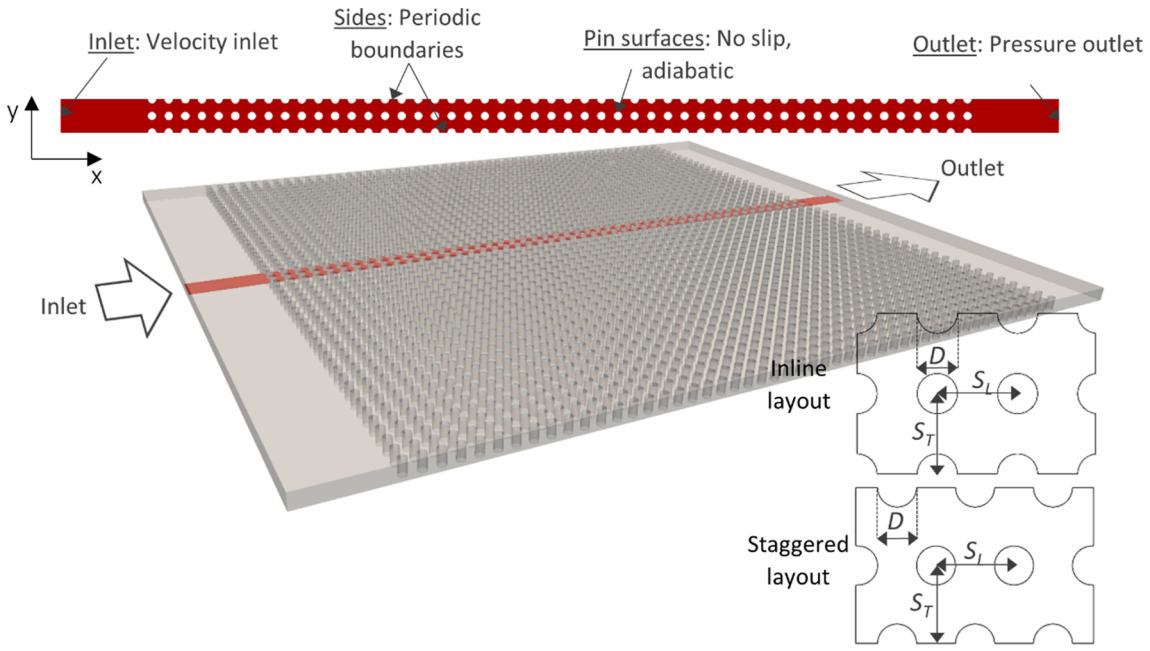

Fig. 1. Physical model and computational domain.

Table 1
Specification of cases.

		Layout	Pin diameter, D, [μm]	Longitudinal spacing, S_L, [μm]	Transverse spacing, S_T, [μm]	Number of pins in the longitudinal direction
Circular	I-D100-Px200-Py200	Inline	100	200	200	50
	I-D90-Px200-Py200	Inline	90	200	200	50
	I-D110-Px200-Py200	Inline	110	200	200	50
	I-D100-Px400-Py200	Inline	100	400	200	25
	I-D100-Px200-Py300	Inline	100	200	300	50
	S-D100-Px200-Py200	Staggered	100	200	200	50
	S-D90-Px200-Py200	Staggered	90	200	200	50
	S-D110-Px200-Py200	Staggered	110	200	200	50
	S-D100-Px400-Py200	Staggered	100	400	200	25
	S-D100-Px200-Py300	Staggered	100	200	300	50

		Layout	Pin diameter (x axis), D, [μm]	Pin diameter (y axis), D, [μm]	Longitudinal spacing, S_L, [μm]	Transverse spacing, S_T, [μm]	Number of pins in the longitudinal direction
Elliptical	I-Dx100-Dy80-Px200-Py160	Inline	100	80	200	160	50
	I-Dx100-Dy60-Px200-Py140	Inline	100	60	200	140	50
	I-Dx100-Dy40-Px200-Py120	Inline	100	40	200	120	50
	I-Dx100-Dy40-Px200-Py60	Inline	100	40	200	60	50
	I-Dx80-Dy100-Px200-Py200	Inline	80	100	200	200	50
	S-Dx100-Dy80-Px200-Py160	Staggered	100	80	200	160	50
	S-Dx100-Dy60-Px200-Py140	Staggered	100	60	200	140	50
	S-Dx100-Dy40-Px200-Py120	Staggered	100	40	200	120	50
	S-Dx100-Dy40-Px200-Py60	Staggered	100	40	200	60	50
	S-Dx80-Dy100-Px200-Py200	Staggered	80	100	200	200	50

Table 2
Perimeter of pins to fluid area.

Case	Relative surface area
D100-Px400-Py200	0.181
D100-Px200-Py300	0.263
Dx80-Dy100-Px200-Py200	0.312
D90-Px200-Py200	0.384
Dx100-Dy80-Px200-Py160	0.410
Dx100-Dy60-Px200-Py140	0.412
Dx100-Dy40-Px200-Py120	0.425
D100-Px200-Py200	0.479
D110-Px200-Py200	0.610
Dx100-Dy40-Px200-Py60	1

Table 3
Inlet velocity values for I-D100-Px200-Py200 and S-D100-Px200-Py200 configurations.

Re_d	u_{inlet} [m/s]
15	0.08
30	0.17
45	0.25
60	0.33
75	0.42
90	0.5
105	0.58
120	0.67
135	0.75
150	0.83
165	0.90
180	1
195	1.08
210	1.17
225	1.25
240	1.33
255	1.41
270	1.5
285	1.58

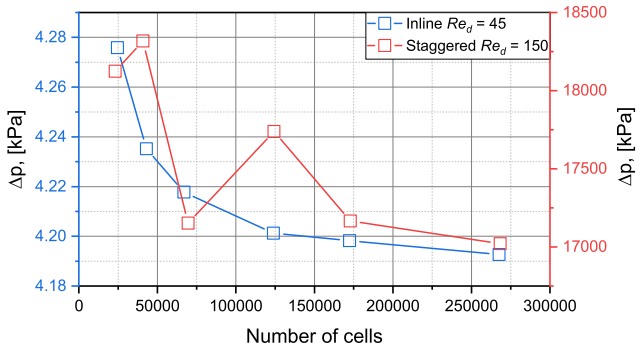

Fig. 2. Grid independence study (D100-Px200-Py200 case).

streamlined fins have the highest thermal performance as well as the lowest pressure drop. The sharp-cornered pin–fin results in a wide wake, which reduces convective heat transfer, while the streamlined pin–fin diminishes wake width, thus enhancing heat transfer because of intense mixing in the wake. Bahiraei et al. [14] carried out numerical research on the effect of circular, triangular, and drop-shaped pin fins on heat transfer. Results showed that the array with the circular fins has lower thermal resistance as well as better efficiency than that with the triangular or drop-shaped fins.

Different research groups have comprehensively explored circular and square pin–fin arrays along with diamond [15,16,17,8,18], ellipse [17,19,20], triangular [17,21,18], hexagon [21], pentagon [21], drop-shape [20,8,18], NACA [20] cross-section shape of the pin-fins. The

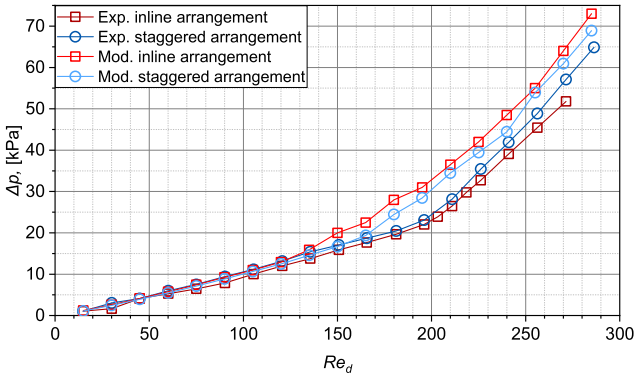

Fig. 3. Comparison of experimental data and numerical results.

sharp edge of the pin fin promotes heat transfer by the flow detachment and induction of more intense turbulence and mixing, while the streamlined pin-fins are aligned up with the flow and are anticipated to have delayed boundary layer separation as well as reduced heat transfer. Nonetheless, Sahiti et al. [20], Yang et al. [19], Izci et al. [18] and Wang et al. [8] examined several significantly different pin–fin shapes, and they all independently agreed that the streamlined pin–fin, whether it may be elliptical, circular or drop-shaped in cross-section, has the best performance compared with the sharp-edged pin–fin. Detailed studies by Mohamed et al. [22] and Wang et al. [23] using different drop-shaped pin–fin dimensions and having Reynolds numbers of 100,000 and 10,000, respectively, reported that variation in pin elongation affected pressure drop more than heat transfer. Sakanova et al. [24] examined streamlined pin–fin shapes like circular, cone, and hydrofoil with the inlet velocity ranging from 0.01 m/s to 8 m/s. They concluded that the highest heat transfer coefficient is achieved by the cone pin–fin array, however, the lowest pressure drop can be achieved by the hydrofoil because there is no flow separation.

Heat transfer and pressure drop characteristics depend not only on the pin–fin shape but also on the layout. The array configuration generally can be sorted into two types – inline and staggered. Moreover, the longitudinal and transverse pin–fin spacing can vary. Xu et al. [25] performed an experimental investigation that estimates the flow transition and hydraulic characteristics of various pin–fin shapes and layouts in the range of Reynolds number of $5 \leq Re < 1010$. They found that the staggered pin–fin microchannels already have wavy flow even before the transition to turbulence, therefore an abrupt pressure drop change was not observed while increasing *Re*, regardless of the shape of the pin–fin. On the contrary, the flow transition can be clearly identified by the sharp change in the pressure drop slope for the inline pin–fin layout. The same trends as in [25], but with respect to the heat transfer performance, were reported by Qiu et al. [9]. As the Reynolds number increases from 79.2 to almost 882.3, a transition point in the increase of Nusselt (*Nu*) number occurs in the case of an inline layout. This is the consequence of a thinner boundary layer and an evolving unsteady Karman vortex street, which was not observed in the staggered array. Reports made by Choudhary et al. [26], Yang et al. [19], Mohammadi et al. [27] indicated that the staggered layout of pin–fin array shows greater heat transfer performance along with higher pressure drop due to frictional losses. However, in all these cases [19,27,26], longitudinal and transverse pin spacing was the same, therefore the flow behind the pin has twice as much space compared to the inline layout.

Furthermore, it was found that the magnitude of the flow velocity fluctuations grows with increasing streamwise spacing as reported by Ostanek et al. [28] considering Reynolds number between $3000 \leq Re \leq 20{,}000$. Further research was conducted by Lawson et al. [29] determining the effect of pin spacing on thermohydraulic characteristics. The ratio of spanwise spacing to diameter (S/D) varied from 2 to 4, while the ratio of streamwise spacing to diameter (X/D) varied from 1.73 to 3.46.

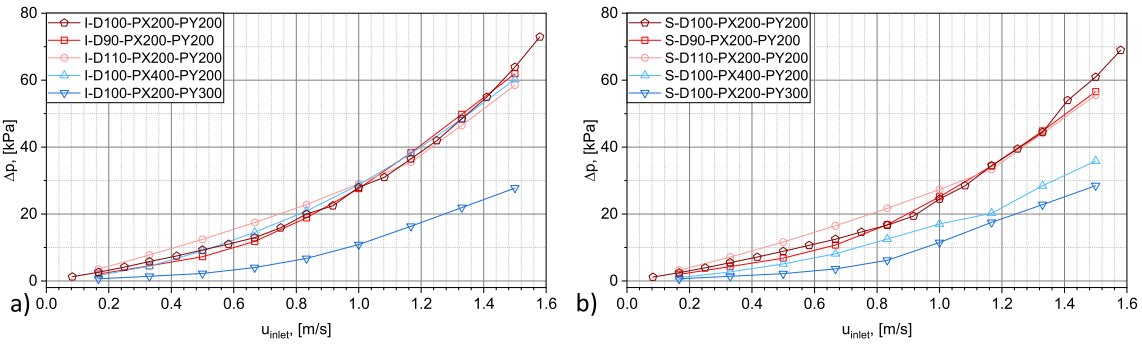

Fig. 4. Pressure drop for different circular pin–fin array configurations: (a) inline, (b) staggered.

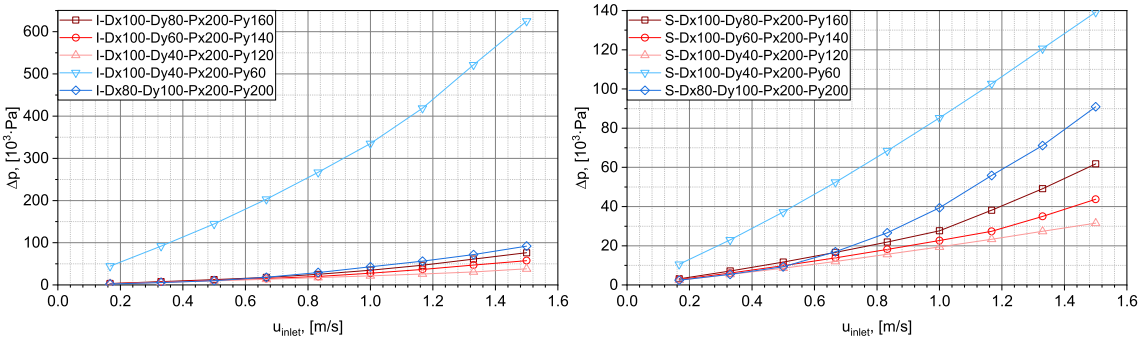

Fig. 5. Pressure drop for different elliptical pin–fin array configurations: (a) inline, (b) staggered.

Table 4
Onset of flow instability in microchannels with circular pin-fins.

u_{inlet}, [m/s]	0.17	0.33	0.5	0.67	0.83	1	1.17	1.33	1.5
I-D100-Px200-Py200	–	–	–	–	III	III	III	II	II
I-D90-Px200-Py200	–	–	–	III	III	II	II	II	II
I-D110-Px200-Py200	–	–	–	–	–	IV	IV	III	III
I-D100-Px400-Py200	–	II	I	I	I	I	I	I	I
I-D100-Px200-Py300	–	–	–	III	III	I	I	I	I
S-D100-Px200-Py200	–	–	–	–	IV	III	III	III	II
S-D90-Px200-Py200	–	–	–	III	III	II	II	II	II
S-D110-Px200-Py200	–	–	–	–	–	–	IV	III	III
S-D100-Px400-Py200	–	–	III	II	I	I	I	I	I
S-D100-Px200-Py300	–	–	–	III	III	I	I	I	I

They found that heat transfer was more dependent on streamwise than on spanwise spacing. Additionally, the thermal performance increases with decreasing spacings. However, the pressure drop increases simultaneously with a stronger dependence on spanwise spacing due to the

Table 5
Description of microchannel sections.

	Pin-fins (if 50 in total)	Distance, mm
I – Beginning	1 to 10	0.001 to 0.003
II – Middle 1	11 to 25	0.003 to 0.006
III – Middle 2	26 to 40	0.006 to 0.009
IV – End	41 to 50	0.009 to 0.011

greater flow blockage. Some other researches confirm and complement previous studies. Jin et al. [30] numerically studied the impact of different shape staggered pin-fins, such as circular, elliptic, oblong, teardrop, and NACA, and investigated the effects of spacing, while Reynolds number varied from 5000 to 30,000. The ratio X/D varied from 2.5 to 5, while the ratio S/D varied from 2 to 4. They concluded that teardrop and NACA fins with $X/D = 2.5$ and $S/D = 3$ were the most efficient. Kirsch et al. [31] experimentally investigated the staggered layout of oblong pins having X/D ratio from 2.16 to 3.13 and S/D ratio from 3 to 4.5 with Reynolds number either 40,000 or 60,000. Reduced streamwise spacings promote heat transfer, but in the staggered layout, the flow characteristics may be altered as it would be suppressed and wakes stabilized.

Prior experimental and numerical studies have documented the effect of pin–fin shape and array configuration on heat transfer at limited geometries, mostly drastically changing pin–fin shape. However, a careful study of the streamlined fins effect on the flow structure and hydraulic characteristics is missing. Furthermore, the unfading research interest in pin array configuration suggests that both layout and spacing may have a significant effect on performance. Although lesser streamwise spacing is more beneficial, most of the studies in the staggered layout have investigated cases with equal or lower spanwise spacings. In general, there are several key factors that determine the efficiency of microchannels: the shape of the pin-fins, the layout, and the spacing. We assume that circular and elliptical pin-fins are the most effective. The effect of layout is ambiguous, but a larger longitudinal distance is more

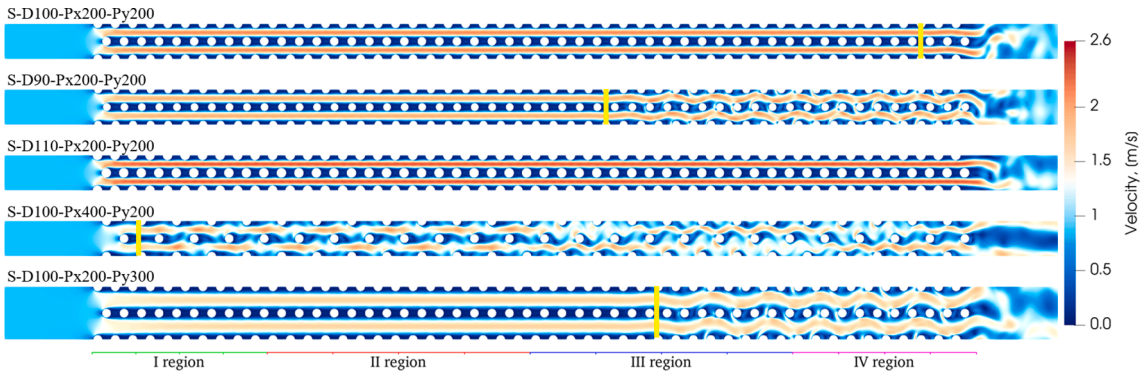

Fig. 6. Velocity profiles of staggered arrays at $u_{inlet} = 0.83$ m/s, yellow markings identify the beginning of vortex shedding. (For interpretation of the references to colour in this figure legend, the reader is referred to the web version of this article.)

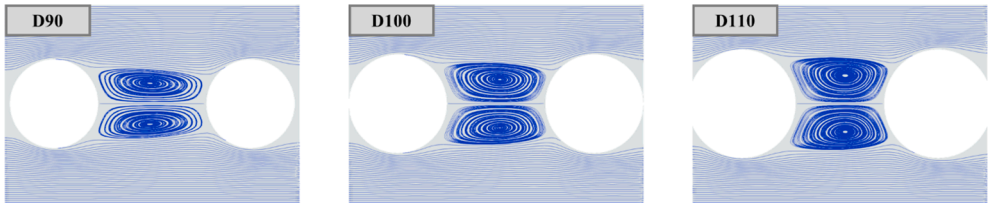

Fig. 7. Streamline distribution for different pin-fins diameter.

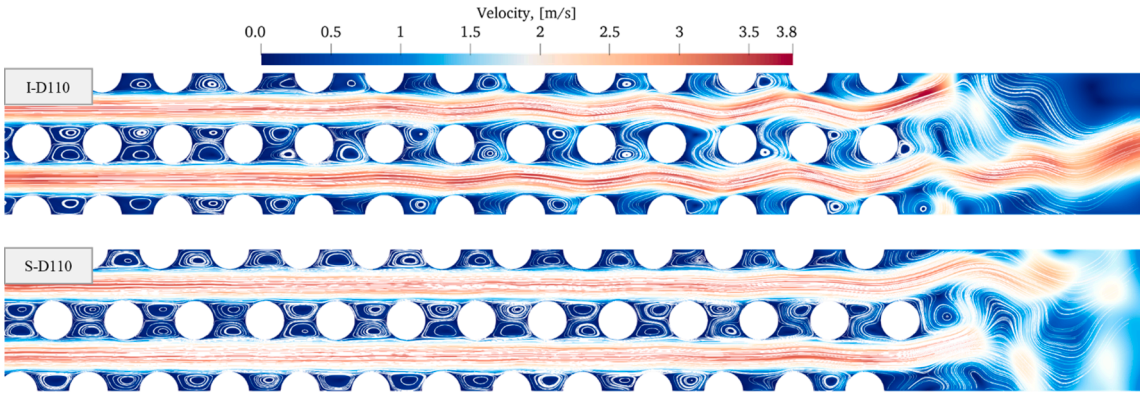

Fig. 8. Velocity profiles with streamlines of D110 configurations at the end of the channel ($u_{inlet} = 1.17$ m/s).

likely to be advantageous than a transverse distance. This work demonstrates a fairly comprehensive, but computationally time-efficient, investigation and comparison of the hydraulic characteristics of 20 different flow cases. Unless the hydraulics is thoroughly investigated, the heat transfer and transport, which depend mainly on it, cannot be well understood. Hence, this paper presents a computational study of the pressure drop and flow structure of microchannels, where the influence of the shape and layout of the pin-fins is examined in depth.

2. Methodology

2.1. Physical model and computational domain

The considered physical model of a square microchannel is a 50×50 array of pin-fins (see Fig. 1), as in an experimental case investigated by Renfer et al. [32]. The layout of the pin-fins was both inline and staggered. The computational domain was simplified up to 2-rows of the pin-fins in the streamwise direction implying a cyclic condition that reduces computational time and saves computer resources. This paper assumes that the effect on pressure drop of obstacles not included in the model is negligibly small. This assumption does not preclude the demonstration of a cost-effective methodology for comparing the performance of micro-channel configurations, allowing for a more informed practical decision. The pin–fin diameter (D), transverse spacing (S_T) and longitudinal spacing (S_L), are 100 μm, 200 μm and 200 μm, respectively. The height of the microchannel was 200 μm, but the considered computational domain is 2D, therefore the effect of the upper and lower walls is not taken into account.

Several modified configurations with different longitudinal/transverse spacing and pin diameter were considered in this paper. There are two different categories of pin–fin geometrical shapes: circular and elliptical. Each case is labelled, and the relative area ratio (*perimeter of pins over flow area*) is calculated accordingly (see Table 1 and Table 2).

2.2. Governing equations, boundary conditions and numerical models

Simulations were performed in *OpenFOAM* software, using the unsteady RANS (U-RANS) method. The flow inside the microchannel is described by solving continuity and conservation of momentum equations:

Table 6
The onset of instability in a flow through microchannel with elliptical pin-fins.

u_{inlet}, [m/s]	0.17	0.33	0.5	0.67	0.83	1	1.17	1.33	1.5
I-Dx100-Dy80-Px200-Py160	–	–	–	–	IV	III	III	II	II
I-Dx100-Dy60-Px200-Py140	–	–	–	–	–	III	III	II	II
I-Dx100-Dy40-Px200-Py120	–	–	–	–	–	–	IV	IV	III
I-Dx100-Dy40-Px200-Py60	–	–	–	–	–	–	I	I	I
I-Dx80-Dy100-Px200-Py200	–	–	IV	III	II	II	II	II	II
S-Dx100-Dy80-Px200-Py160	–	–	–	–	–	–	III	III	III
S-Dx100-Dy60-Px200-Py140	–	–	–	–	–	–	–	III	III
S-Dx100-Dy40-Px200-Py120	–	–	–	–	–	–	–	–	–
S-Dx100-Dy40-Px200-Py60	–	–	–	–	–	–	–	–	–
S-Dx80-Dy100-Px200-Py200	–	–	IV	III	II	II	II	II	II

$$\frac{\partial \overline{u_i}}{\partial x_i} = 0 \tag{1}$$

$$\frac{\partial}{\partial t}\overline{u_i} + \frac{\partial}{\partial x_j}\left(\overline{u_i u_j} + \rho\overline{u'_i u'_j}\right) = \frac{\partial \overline{\tau}_{ij}}{\partial x_j} - \frac{1}{\rho}\frac{\partial \overline{p}}{\partial x_i} + f_i \tag{2}$$

where: u– velocity, t – time, p – pressure,τ – shear-rate tensor, f_i – external forces.

The k-ω SST turbulence model [33] was used to simulate the flow in a pin–fin array as it has been validated as a proper model for complex flows similar to our case [34,35,36,37,38,39,40], as the main focus and objective of turbulence models is to give a "closure" to the RANS equations. Fluid was assumed to be incompressible, isothermal, Newtonian with constant physical properties. Velocity and pressure coupling between momentum and continuity equations was governed by PIMPLE algorithm. The second order linearUpwind scheme is used for the momentum discretization, and limitedLinear scheme is used for the turbulence model equations. The Euler scheme was selected for temporal discretization. The time step was automatically adjusted to maintain Courant-Friedrichs-Lewy (CFL) number at an approximately constant value of one. The 10^{-5} convergence criterion has been applied to the computing all governing equations. Computing a single case at 160 GFLOPS (12 processors), depending on the number of *Re*, took about an hour to half a day at most.

In the present numerical work as shown in Fig. 1, water at constant temperature (289.15 K) enters the domain at a uniform inlet velocity, which was determined by the Reynolds number to be consistent with each experiment (relation of Re_d and u_{inlet} can be seen in Table 3):

$$Re_d = \frac{u_m D}{\nu} \tag{3}$$

where: ν – kinematic viscosity, u_m – mean velocity of the fluid between pin-fins, which can be calculated as:

$$u_m = \frac{\dot{V}}{H(S-D)N_p} \tag{4}$$

where: H – channel height, S – pin spacing, N_p – number of pins in a cross-section normal to the flow direction.

All walls were treated as adiabatic with the no-slip condition, except periodic boundaries. The outlet pressure was set to atmospheric pressure.

2.3. Model validation and grid independence

In this study, a structured grid system with hexahedron elements was employed to fulfil the complex microchannel configurations. Initial simulations were performed to determine the grid resolution needed for mesh-independence. y^+ values of <1 are achieved at all walls of the microchannel in order to meet the requirements for wall approximation and to resolve the flow up to the wall, for example, when $Re_d = 195$ average valueof the y^+ was 0.58 and at $Re_d = 195$ y^+ it reached 0.826.

Grid independence study was tested for I-D100-Px200-Py200 and S-D100-Px200-Py200 cases, having $Re_d = 45$ and 150, respectively. Several different grids (with an average cell size of $13{\cdot}10^{-6}$ m, $10{\cdot}10^{-6}$ m, $8{\cdot}10^{-6}$ m, $6{\cdot}10^{-6}$ m, $5{\cdot}10^{-6}$ m and $4{\cdot}10^{-6}$ m) were used to determine the dependence of the solution on the grid resolution, with 24620, 43060, 66900, 123912, 172,400 and 267,600 cells in a inline layout and with 23180, 40814, 69600, 124252, 172,880 and 268,300 cells in a staggered layout, respectively. Fig. 2 shows the convergence results in terms of pressure drop. It can be seen that grid of $5{\cdot}10^{-6}$ m cells is sufficient to obtain accurate and invariant pressure drop values, as there is no significant change as with increasing grid. For example, the difference between $5{\cdot}10^{-6}$ m and $4{\cdot}10^{-6}$ m is <1 % and 0.24 % for staggered layout with $Re_d = 150$ and inline layout with $Re_d = 45$. Therefore, meshes with an average cell size of $5{\cdot}10^{-6}$ m were used for further investigation.

A comparison of the experimental and simulated pressure drop results represents the validation for the accuracy of the modelled flow. The pressure was probed along the fluid path before the first pin and after the last, pressure ports were located in the cavity, so there may be some pressure deviations as it is modelled differently than measured. The results of I-D100-Px200-Py200 and S-D100-Px200-Py200 configurations were compared with the experimental data of Renfer et al. [32]. Fig. 3 shows the evolution of the dependence of the pressure drop on Re_d. The agreement between the experimental data and the modelling results is confirmed to be acceptable. The main difference comes from the exclusion of the upper and lower walls, which resulted in a faster transition to turbulence, whereas in the experiment these walls stabilised the flow. Furthermore, in contrast to the experiment, the pressure drop in the staggered layout is higher than in the inline layout. This result can also be explained by the 2D model. Taller channel results in a higher pressure drop as well as increased wake shedding [41]. The deviation of the inline array simulation results from experimental results has larger than that of the staggered array; in the region $15 \leq Re_d \leq 150$, the deviations are 13 % and 7 %, respectively. In the further region ($150 < Re_d \leq 270$ for inline and $150 < Re_d \leq 285$ for staggered), the deviations are 23 % and 10 %. The average deviation of pressure drop is a little bit higher than 10 %. Consequently, the error between the experimental and modelled data is considered acceptable, which means that the numerical model of the present study is reliable. Also, further modelling of different configurations will be represented by means of inlet velocity.

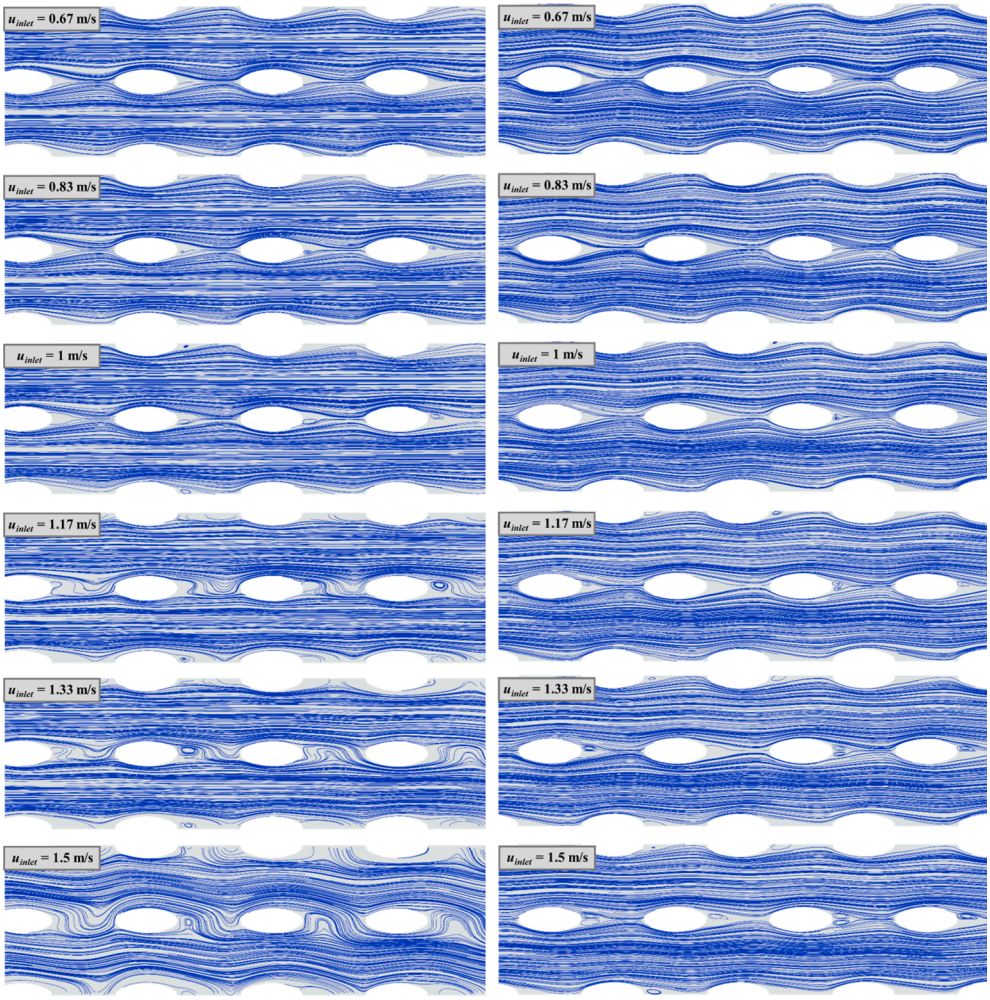

Fig. 9. Streamlines of flow through Dy40-Py120 microchannels with the inline and staggered layout.

3. Results and discussion

This study evaluates the effect of pin diameter, transverse/longitudinal spacing in arrays with different layouts, including circular and elliptical fins, on hydraulic features. The results of pressure drop and instability onset are presented to illustrate the influence of differences in pin–fin arrays. Furthermore, the streamlines are shown to elaborate flow characteristics.

3.1. Hydrodynamic characteristics

Fig. 4 and Fig. 5 show the pressure drops in microchannels with an inline and staggered layout and with circle and ellipse shape pin-fins, respectively. All cases presented show an increasing trend in pressure drop with increasing inlet velocity value. Nonetheless, D100-Px200-Py300 has the lowest pressure drop gradient, which can be associated with the highest transverse spacing and one of the lowest heat dissipation area. Thus, the flow at larger transversal than the longitudinal spacings becomes more like flow between two plates, where pressure drop is lower. It can be noted that D100-Px400-Py200 also has a low pressure drop, however, this is only the case when the layout is staggered. In the case of inline layout, the drop is similar to the other cases. Such behaviour can be associated with one of the fastest transitions to turbulence.

Despite the fact that pin-fins with streamlined shape are considered to be the most effective, the cases studied in this work show that elliptical pin-fins are not always the most effective. Moderately narrower transverse spacing between the pins results in a huge pressure drop (see Fig. 5 Py60), which is lower even when the shape is non-streamlined (Dx80-Dy100). For example, the pressure drop of Dx100-Dy40 with Py60 is 10 times higher than Py120, whereas the surface area to volume ratio of Py60 case is only 2.35 times higher. A notable reduction of pressure drop can be attributed to a more stable flow, which reduces the overall interaction between the fluid and pin-fins, which is also diminished by staggered layout.

The lowest pressure drops were achieved in elliptical Dx100-Dy40-Py200-Py120 and circular D100-Px200-Py300 pin–fin configurations. The former has an average pressure drop of 1.6 times that of the latter, but also surface area-to-volume ratio of 1.68 times.

3.2. Occurrence of flow transition

This section highlights the fluid flow characteristics that depend on the shape of the pin–fin, in terms of streamlines, velocity contours and the onset of instability.

3.2.1. Effects of circular pin fins

Table 4 outlines the onset of flow instability. Roman numerals denote sections of the channel (see Table 5), the region after all pins does not count. In general, the onset of instability indicates whether or not the recirculation zone is stagnant, in other words, whether or not vortex shedding has started between the pins. As the flow becomes unsteady, vortex shedding starts, which improves mixing but also increases the pressure drop. A steady pair of vortices behind the pins indicates that the

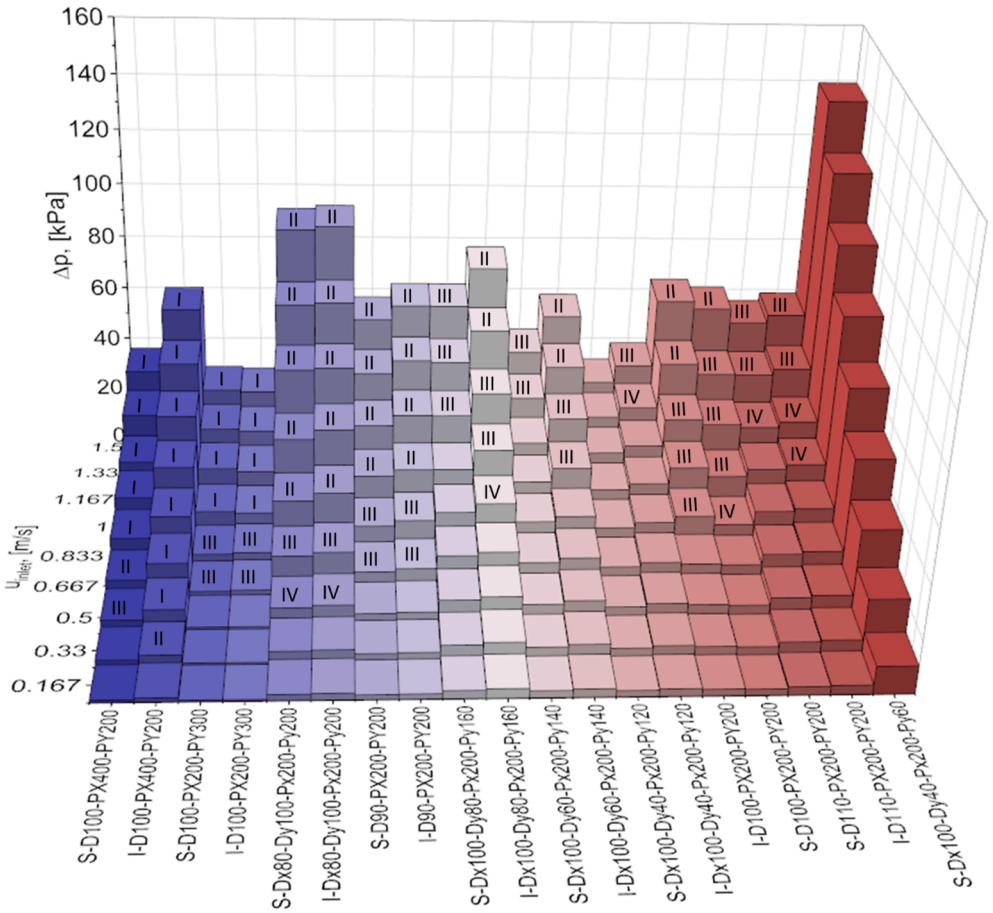

Fig. 10. Pressure drop dependence on u_{inlet} and configuration.

flow is laminar, but as the u_{inlet} increases the flow loses stability. A vortex street is formed when the *Re* reaches a critical value [42]. Therefore, alternating symmetric vortex shedding occurs, which is a natural instability in the transition from laminar to turbulent flow. An example of region identification at $u_{inlet} = 0.83$ m/s is shown in Fig. 6 and the yellow lines indicate the location in the channel where vortex shedding starts.

The diameter, spacing and layout of the array of the pins affected the flow transition. It is related to vortex shedding, which causes transverse velocity fluctuations. Larger diameter pins lead to a more stable flow, as can be seen in Table 4. The widest, but also the shortest, double vortices formed behind the pin fins in D110 case (See Fig. 7). The most relevant research focuses on changing the spacing while keeping the diameter the same, but in that case, the width of the wake remains the same and only the length of double vortices changes [43]. Therefore, the slope of the pressure drop is almost the same for different longitudinal spacing [29,44].

D110 array has one of the highest effective heat transfer areas (see Table 2) with larger vortices as the flow becomes unstable. Also, this case has the lowest slope Δp, i.e., at low Red the pressure drop is highest, but as u_{inlet} increases, the pressure drop becomes lower than in other cases. John et al. [45] concluded that an increase in cylinder diameter in an inline array results in the increase of pressure drop. On the other hand, their simulation results shows the same pressure trend in the entire *Re* range studied ($50 < Re < 500$), which was conducted at steady-state, while our results show a changing trend after the flow undergoes vortex shedding. For example, for D90 case the pressure drop values were lowest up to $u_{inlet} \sim 0.83$ m/s, but after that the slope increased and then for D110 case the pressure drop was the lowest. Even though recirculation regions in Fig. 7 occupy a very similar area (only 2 % difference), the wider vortices downstream of the pin-fins are more resistant to deflection towards the main flow, thereby causing a delayed vortex shedding.

Both the wider transverse and longitudinal spacing between the pins lead to an earlier transition to turbulence. Despite this, the pressure drop is also lower, for example, in the cases with Py300 the pressure drop is the lowest independently of the layout, while for Px400 is only lower in the cases with the staggered layout. Additionally, all staggered layouts require longer or at least the same path for transition to turbulence, as well as lower pressure drop, compared to the corresponding inline layouts. Consequently, more densely spaced and staggered arrays are more effective.

Also, it can be stated that large periodic changes in the cross-sectional area of the flow have a greater influence on the flow regime than the meandering of the flow path. Thus, in inline layouts, the flow is more unstable, while in staggered layouts entrainment of recirculation zones in the main flow prevents the formation of stagnant vortices and moderates pressure drops. For example, the onset of instability for D110 starts in section IV (see Table 4). Nonetheless, as can be seen in Fig. 8, the flow becomes unstable at the 11-th row of pin-fins from the channel end in the inline layout and only at the 6-th row in staggered. It may be attributed to the greater acceleration of the fluid between adjacent pin-fins in the inline layout, which promotes turbulence.

3.2.2. *Effects of elliptical pin fins*

Table 6 presents the onset of flow instability in an array of elliptical pin-fins. A comparison of the transition to turbulence in circular and elliptical pin–fin configurations (see Table 4 and Table 6), as expected, confirms that the streamlined obstacles result in a more stable flow.

Fig. 9 clearly shows that in Dy40-Py120 case, vortices stay attached

up to a relatively high inlet velocity value. As the u_{inlet} is further increased, there is no obvious flow separation in the staggered layout up to $u_{inlet} = 1$ m/s, when very small vortices start to form. While the double vortex wake forms closer to the inlet in the inline layout, where the vortex shedding occurs at $u_{inlet} = 1.17$ m/s. In contrast, vortex shedding in the staggered layout does not occur over the entire range of u_{inlet} investigated. This result confirms that changes in the cross-sectional area of the flow promote turbulence, while changes in the direction of the flow of the same cross-sectional area reduce the tendency for wakes to be drawn into the main flow.

The least stable flow is in Dx80 case, it can be explained by the non-streamlined shape, which causes separation effects and leads to better mixing. It is not surprising that pressure drop, in this case, is one of the highest, but Dx100-Dy40-Px200-Py60 surpasses it not only by a higher pressure drop in both layouts but also by a more stable flow. Such high pressure drop and flow stability in the case of Dx100-Dy40-Px200-Py60 are due to confined flow conditions, where local transverse pressure gradients are weak compared to longitudinal ones. Therefore, the main flow does not entrain stagnant vortices, persisting behind the pin-fins. This confirms that the flow path has a great effect on the occurrence of instabilities in microchannels.

3.3. Overall performance

The previous sections pressure drop and flow regime in different microchannel configurations were discussed. Because both are important for the performance of hypothesized microchannel, their proper balance is a design optimization problem for the pin–fin array. Not every elliptical pin–fin configuration was more efficient than the standard circular pin–fin geometry due to the excessive pressure drop.

Fig. 10 illustrates the dependence of the pressure drop on u_{inlet} for every configuration considered. Cases are lined up by the effective surface area to volume ratio, starting with the smallest from the left (I-Dy40-Py60 is not shown because of the enormous pressure drop). Comparing pairs of configurations with the different layouts shows that the staggered layout generally has lower pressure drop as well as better stability. It can be seen that the S-Dx100-Dy40-Px200-Py120 configuration is the most efficient of those tested due to its stable flow and one of the lowest pressure drops.

4. Conclusions

In this numerical research, the flow in the microchannel was modelled. The hydrodynamic performance of 20 different inline and staggered layouts with circular or elliptical pin-fins was examined and compared. Pin-fin array parameters, such as transverse and longitudinal spacing, diameter and arrangement, affected the flow regime and pressure drop. The findings of this study can be summarized as follows:

- The diameter of the pin-fins affects the strength of vortices formed behind them. The larger diameter results in wider and more stable wakes, reducing the slope of Δp at higher u_{inlet}. Smaller diameter pins create long and narrow vortex pairs which get stronger shedding and the flow is less stable.
- A shorter spacing generally results in a higher pressure drop. Nonetheless, a narrower transverse spacing should be considered, because, besides a larger surface area to volume ratio, it stabilizes the flow.
- Flow is less stable in arrays with an inline layout. This is attributed to changes in the cross-sectional area, which has a greater influence than flow diversions.
- Of all the configurations investigated, the S-Dx100-Dy40-Px200-Py120 case was discovered as the best set of parameters for the microchannels. Its vorticity is very low and the pressure drop is one of the lowest.

Declaration of Competing Interest

The authors declare that they have no known competing financial interests or personal relationships that could have appeared to influence the work reported in this paper.

References

[1] Z. He, Y. Yan, Z. Zhang, Thermal management and temperature uniformity enhancement of electronic devices by micro heat sinks: a review, Energy 216 (2021) 119223, https://doi.org/10.1016/j.energy.2020.119223.
[2] Z. Khattak, H.M. Ali, Air cooled heat sink geometries subjected to forced flow: a critical review, Int. J. Heat Mass Transf. 130 (2019) 141–161.
[3] I.A. Ghani, N.A.C. Sidik, N. Kamaruzaman, Hydrothermal performance of microchannel heat sink: the effect of channel design, Int. J. Heat Mass Transf. 107 (2017) 21–44.
[4] Z. He, Y. Yan, S. Feng, X. Li, Z. Yang, Numerical study of thermal enhancement in a micro-heat sink with ribbed pin-fin arrays, J. Therm. Anal. Calorim. 143 (3) (2021) 2163–2177.
[5] C.H.K. Williamson, Vortex dynamics in the cylinder wake, Annu. Rev. Fluid Mech. 28 (1) (1996) 477–539.
[6] A. Žukauskas, Heat transfer from tubes in crossflow, in: Advances in Heat Transfer, Elsevier, 1972, pp. 93–160.
[7] F. Alfieri, M.K. Tiwari, A. Renfer, T. Brunschwiler, B. Michel, D. Poulikakos, Computational modeling of vortex shedding in water cooling of 3D integrated electronics, Int. J. Heat Fluid Flow 44 (2013) 745–755.
[8] P. Wang, L. Chen, Thermal and hydraulic performance of micro pin fin heat sinks with different pin fin shapes, IOP Conf. Ser.: Mater. Sci. Eng. 542 (1) (2019) 012053, https://doi.org/10.1088/1757-899X/542/1/012053.
[9] Y. Qiu, W. Hu, C. Wu, W. Chen, An experimental study of microchannel and micro-pin-fin based on-chip cooling systems with silicon-to-silicon direct bonding, Sensors 20 (19) (2020) 5533, https://doi.org/10.3390/s20195533.
[10] S. Gasiunas, M. Seporaitis, K. Almenas, Turbulence predicting criterion based on shear forces at the boundaries in a two-phase flow, Int. J. Therm. Sci. 135 (2019) 61–71.
[11] T. Ambreen, M.-H. Kim, Effect of fin shape on the thermal performance of nanofluid-cooled micro pin-fin heat sinks, Int. J. Heat Mass Transf. 126 (2018) 245–256.
[12] T. Ambreen, A. Saleem, H.M. Ali, S.A. Shehzad, C.W. Park, Performance analysis of hybrid nanofluid in a heat sink equipped with sharp and streamlined micro pin-fins, Powder Technol. 355 (2019) 552–563.
[13] T. Ambreen, A. Saleem, C.W. Park, Pin-fin shape-dependent heat transfer and fluid flow characteristics of water-and nanofluid-cooled micropin-fin heat sinks: square, circular and triangular fin cross-sections, Appl. Therm. Eng. 158 (2019) 113781, https://doi.org/10.1016/j.applthermaleng.2019.113781.
[14] M. Bahiraei, S. Heshmatian, M. Goodarzi, H. Moayedi, CFD analysis of employing a novel ecofriendly nanofluid in a miniature pin fin heat sink for cooling of electronic components: effect of different configurations, Adv. Powder Technol. 30 (11) (2019) 2503–2516.
[15] M.K. Chyu, C.H. Yen, S. Siw, Comparison of heat transfer from staggered pin fin arrays with circular, cubic and diamond shaped elements, in: Turbo Expo: Power for Land, Sea, and Air, 2007, pp. 991–999.
[16] P. Dupuis, Y. Cormier, M. Fenech, B. Jodoin, Heat transfer and flow structure characterization for pin fins produced by cold spray additive manufacturing, Int. J. Heat Mass Transf. 98 (2016) 650–661.
[17] J. Hua, G. Li, X. Zhao, Q. Li, J. Hu, Study on the flow resistance performance of fluid cross various shapes of micro-scale pin fin, Appl. Therm. Eng. 107 (2016) 768–775.
[18] T. İzci, M. Koz, A. Koşar, The effect of micro pin-fin shape on thermal and hydraulic performance of micro pin-fin heat sinks, Heat Transfer Eng. 36 (17) (2015) 1447–1457.
[19] K.-S. Yang, W.-H. Chu, I.-Y. Chen, C.-C. Wang, A comparative study of the airside performance of heat sinks having pin fin configurations, Int. J. Heat Mass Transf. 50 (23-24) (2007) 4661–4667.
[20] N. Sahiti, F. Durst, P. Geremia, Selection and optimization of pin cross-sections for electronics cooling, Appl. Therm. Eng. 27 (1) (2007) 111–119.
[21] D. Yang, Y. Wang, G. Ding, Z. Jin, J. Zhao, G. Wang, Numerical and experimental analysis of cooling performance of single-phase array microchannel heat sinks with different pin-fin configurations, Appl. Therm. Eng. 112 (2017) 1547–1556.
[22] A.A. Mohamed, O. Younis, Performance of drop shaped pin fin heat exchanger with four different fin dimensions, J. Mech. Eng. Sci. 14 (2) (2020) 6934–6951.
[23] F. Wang, J. Zhang, S. Wang, Investigation on flow and heat transfer characteristics in rectangular channel with drop-shaped pin fins, Propul. Power Res. 1 (1) (2012) 64–70.
[24] A. Sakanova, K.J. Tseng, Comparison of pin-fin and finned shape heat sink for power electronics in future aircraft, Appl. Therm. Eng. 136 (2018) 364–374.
[25] F. Xu, Z. Pan, H. Wu, Experimental investigation on the flow transition in different pin-fin arranged microchannels, Microfluid. Nanofluid. 22 (1) (2018), https://doi.org/10.1007/s10404-017-2030-4.
[26] V. Choudhary, M. Kumar, A.K. Patil, Experimental investigation of enhanced performance of pin fin heat sink with wings, Appl. Therm. Eng. 155 (2019) 546–562.

[27] A. Mohammadi, A. Koşar, The effect of arrangement type and pitch ratio on the performance of micro-pin-fin heat sinks, J. Therm. Anal. Calorim. 140 (3) (2020) 1057–1068.
[28] Jason K. Ostanek, Karen A. Thole, Effects of non-uniform streamwise spacing in low aspect ratio pin fin arrays, in: Turbo Expo: Power for Land, Sea, and Air. American Society of Mechanical Engineers, 2013, pp. V03AT12A050.
[29] S.A. Lawson, A.A. Thrift, K.A. Thole, A. Kohli, Heat transfer from multiple row arrays of low aspect ratio pin fins, Int. J. Heat Mass Transf. 54 (17-18) (2011) 4099–4109.
[30] W. Jin, J. Wu, N. Jia, J. Lei, W. Ji, G. Xie, Effect of shape and distribution of pin-fins on the flow and heat transfer characteristics in the rectangular cooling channel, Int. J. Therm. Sci. 161 (2021) 106758, https://doi.org/10.1016/j.ijthermalsci.2020.106758.
[31] K.L. Kirsch, K.A. Thole, Heat transfer measurements of oblong pins, J. Turbomach. 137 (7) (2015), https://doi.org/10.1115/1.4029124.
[32] A. Renfer, M.K. Tiwari, T. Brunschwiler, B. Michel, D. Poulikakos, Experimental investigation into vortex structure and pressure drop across microcavities in 3D integrated electronics, Exp. Fluids 51 (3) (2011) 731–741.
[33] Menter, R. Florian, Two-equation eddy-viscosity turbulence models for engineering applications, AIAA J. 32 (8) (1994) 1598–1605.
[34] O. Bovati, M.A. Yildiz, Y. Hassan, R. Vaghetto, RANS simulations for transition and turbulent flow regimes in wire-wrapped rod bundles, Int. J. Heat Fluid Flow 90 (2021) 108838, https://doi.org/10.1016/j.ijheatfluidflow.2021.108838.
[35] D. Dovizio, B. Mikuž, A. Shams, F. Roelofs, Validating RANS to predict the flow behavior in wire-wrapped fuel assemblies, Nucl. Eng. Des. 356 (2020) 110376, https://doi.org/10.1016/j.nucengdes.2019.110376.
[36] D.i. Zhang, Comparison of various turbulence models for unsteady flow around a finite circular cylinder at Re= 20000, IOP Publishing, J. Phys.: Conf. Ser. 910 (2017) 012027, https://doi.org/10.1088/1742-6596/910/1/012027.
[37] Royce Fernandes, Mark A. Ricklick, CFD benchmarking of heat transfer and pressure drop predictions in a pin fin channel, in: 51st AIAA/SAE/ASEE Joint Propulsion Conference, 2015, pp. 3736.
[38] R. Fernandes, M. Ricklick, A. Prasad, Y. Pai, Benchmarking reynolds averaged navier–stokes turbulence models in internal pin fin channels, J. Thermophys. Heat Transf. 31 (4) (2017) 976–982.
[39] Li. Weihong, et al., Assessment of six turbulence models for modeling and predicting narrow passage flows, Part 2: Pin fin arrays, Numer. Heat Transf. Part A: Appl. 69 (5) (2016) 445–463.
[40] Noora Imad Haseeb Algburi, Hayati Kadir Pazarlioğlu, Kamil Arslan, Effect of pitch ratio and diagonal length of pin fin of heat sink on convective heat transfer for turbulent flow condition. *Avrupa Bilim ve Teknoloji Dergisi*, vol. 28, 2021, pp. 643–652.
[41] Minking K. Chyu, Sean C. Siw, Hee Koo Moon, Effects of height-to-diameter ratio of pin element on heat transfer from staggered pin-fin arrays, in: Turbo Expo: Power for Land, Sea, and Air, 2009, pp. 705–713.
[42] c.p. Jackson, A finite-element study of the onset of vortex shedding in flow past variously shaped bodies, J. Fluid Mech. 182 (1987) 23–45.
[43] Jason K. Ostanek, Karen A. Thole, Effects of varying streamwise and spanwise spacing in pin-fin arrays, in: Turbo Expo: Power for Land, Sea, and Air. American Society of Mechanical Engineers, 2012, pp. 45–57.
[44] Mustafa Koz, Ali Kosar, Parameter optimization of a micro heat sink with circular pin-fins, In: International Conference on Nanochannels, Microchannels, and Minichannels, 2010, pp. 531–539.
[45] T.J. John, B. Mathew, H. Hegab, Parametric study on the combined thermal and hydraulic performance of single phase micro pin-fin heat sinks Part I: Square and circle geometries, Int. J. Therm. Sci. 49 (11) (2010) 2177–2190.